Atomistic simulations of strain distributions in quantum dot nanostructures

2003 J. Phys.: Condens. Matter 15 133

(http://iopscience.iop.org/0953-8984/15/2/313)

INSTITUTE OF PHYSICS PUBLISHING JOURNAL OF PHYSICS: CONDENSED MATTER

J. Phys.: Condens. Matter **15** (2003) 133–146 PII: S0953-8984(03)52096-3

Atomistic simulations of strain distributions in quantum dot nanostructures

Christopher Kohler

Institut für Theoretische und Angewandte Physik, Universität Stuttgart, D-70550 Stuttgart, Germany

E-mail: kohler@itap.physik.uni-stuttgart.de

Received 7 August 2002
Published 20 December 2002
Online at stacks.iop.org/JPhysCM/15/133

Abstract

Strain distributions around a Ge quantum dot (QD) buried in a Si spacer layer are investigated theoretically by means of classical molecular dynamics simulations using the Tersoff potential. Applying periodic boundary conditions laterally, two-dimensional superlattices of QDs are obtained. Strain distributions in systems of different sizes and lattice misorientations are computed in order to explain possible vertical correlations in self-organized three-dimensional QD superstructures. Generally, the strain of relaxed systems displays an oscillatory behaviour as a function of the distance from the QD. For QD systems with growth direction [001], a simple fitting function is used to describe the strain along a vertical path above the QD by an oscillation and a decay according to a power law. For QDs with the shape of a truncated pyramid, the planar strain decays by a power of approximately -3. The period of the oscillation is nearly proportional to the QD superlattice constant and decreases with increasing coordination number of the QD superlattice. In misoriented systems with a small tilt angle about the [110] axis, the region of tensile planar strain above the QD is bent in the direction opposite to the misorientation causing a vertical correlation with lateral shift. For a tilt angle $\approx 55°$, no strain oscillation is found which implies a perfect vertical correlation.

1. Introduction

Three-dimensional superstructures of self-assembled semiconductor quantum dots (QDs) are being intensively investigated currently because of their promising applications in optoelectronic devices. The vertical self-ordering in the heteroepitaxial growth of QD superlattices is generally attributed to the strain fields of the QDs buried in a spacer layer (SL). Due to the lattice mismatch between the dot material and the matrix material, QDs preferentially nucleate at those positions on the wetting layer (WL) covering the SL where the strain is enlarged. Various correlations of QDs in consecutive layers have been observed:

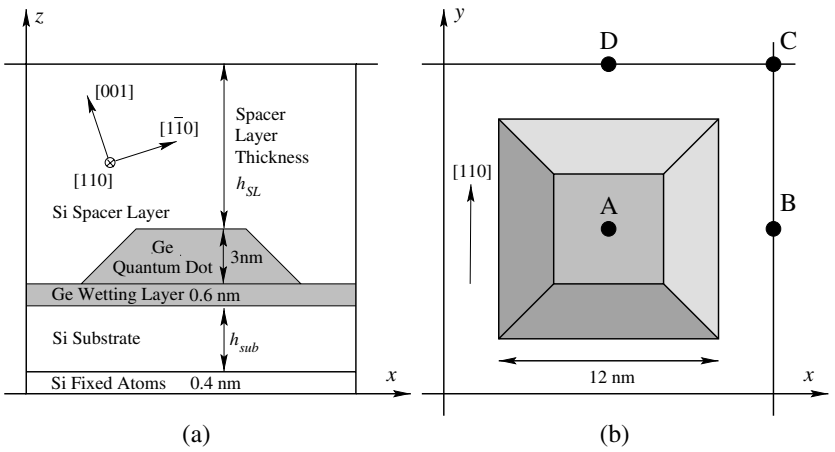

Figure 1. Schematic illustration of the simulation box. (a) Vertical section through the middle of the box. (b) View from above with the location of four vertical paths.

perfect vertical alignment [1], vertical anticorrelation with different stackings [2, 3] and vertical correlation with lateral shift in the case of misoriented samples [4]. It has been demonstrated by continuum elasticity calculations [5, 6] that all these correlations can be explained by the elastic anisotropy of the matrix material. These calculations, however, partly use simplified geometries of the QD system along with approximations and therefore do not provide a detailed insight into the strain fields in the vicinity of the QDs.

In order to obtain the strain distributions in systems of QDs of realistic size, atomistic simulations with empirical interatomic potentials are a convenient method. These have been used in several recent investigations. For Ge QDs in a Si matrix with growth direction [001], strain profiles [7] and hydrostatic stress profiles [8] have been determined for systems of several sizes, surface stress distributions for a stacking of QDs have been given [9] and the hydrostatic stress and strain have been computed for uncapped QDs [10]. For a system of InAs/GaAs QDs with growth direction [001], a comparison of calculations of strain distributions by means of continuum and atomistic methods has been given [11]. Systems of CdSe/ZnSe QDs have been considered [12], and in the case of InP/GaInP QDs simulated strain distributions have been compared with experimentally determined ones [4].

In this work, results of simulations of strain distributions in Ge/Si QD systems are presented with a special focus on the vertical correlations caused by the strain. The Ge/Si system can be considered as a model system for semiconductors with cubic symmetry. Simulations have been performed with a large variation of the lateral and vertical system sizes. Furthermore, QD systems with growth directions different from the [001] direction have also been studied. While in the previous investigations the Stillinger–Weber potential [4, 7–10, 12] and the Keating potential [7, 11] have been used, the Tersoff potential is employed in the present work. In order to simulate strain distributions, it is important that the potential accurately reproduces the elastic properties. It has been shown that the Tersoff potential is superior to other many-body potentials in this respect [13].

This article is organized as follows. In section 2, the simulation method is described. In section 3, the results of simulations are discussed for systems of QDs with several growth directions corresponding to misorientation angles 0°, 13.26°, 54.74° and 90°. Section 4 contains a summary and conclusions.

2. Method of simulation

Silicon and germanium are covalent crystals which possess the diamond structure. In order to model these systems by classical molecular dynamics simulations, many-body potentials have to be used which allow for the simulation of directed bonds. In this article, the Tersoff potential is employed in the form given by [14].

The simulation box consists of a single Ge QD embedded in a Si matrix. A vertical section through the starting configuration is shown schematically in figure 1(a). The systems have a Si substrate of height h_{sub} below which a bottom layer of height 4 Å is held fixed during the simulations. Above the substrate is a thin WL of Ge atoms with fixed height of 6 Å corresponding to five monolayers if the layer plane is along (001). While this is within the range found experimentally [15], the simulated strain distributions above the QD are nearly independent of the thickness of the WL. The QD consists of a truncated quadratic pyramid of Ge atoms the base length of which is 12 nm. Many shapes of QDs have been found experimentally [16]. The inclination of the sidewalls of the dot is chosen in this work to be 45° with respect to the z-axis. The truncation is performed at half the height of the corresponding pyramid, that is, at height 3 nm. The dot is covered by a Si SL of thickness h_{SL}. The y-axis of the box is always the [110] direction while the [001] direction is tilted against the z-axis by the angle θ in the case of misoriented systems. Periodic boundary conditions are applied in the x- and y-directions implying that the systems effectively consist of infinite two-dimensional superlattices of QDs. At the top of the SL, free boundary conditions are used. Figure 1(b) shows a schematic view of the simulation box from above. The points A, B, C and D are the positions of four vertical paths (or, more precisely, tubes) along which the strain profiles will be studied in detail. In the case of the misorientation angle 0°, the paths B and D are equivalent. The base plane is chosen to be quadratic, or nearly quadratic in the case of misoriented systems. Simulations are performed for base lengths from 18 to 50 nm and for box heights from 14 to 40 nm. Correspondingly, the number of atoms in the box varies from some hundred thousand to some million atoms. In order to test the influence of the chosen box geometry on the strain distribution, simulations with configurations different from the ones described above have also been performed.

In this paper, we are interested in the strain distribution of the relaxed systems. The relaxation is performed in a molecular dynamics simulation by setting the velocities of all atoms to zero whenever the system moves out of a potential minimum, that is, when the scalar product of the force vector and the momentum is negative. In the final state, the mean force on the atoms is lower than 10^{-8} eV Å^{-1}. The strain of the relaxed systems consists of two contributions, one originating from the free surface of the SL and one from the lattice mismatch of the QD and the WL. Since we are interested here in the latter part only, the systems are relaxed in two steps. First, the systems without the WL and QD are relaxed, that is, the atoms of the WL and QD are taken to be Si atoms. Then, the Ge atoms of the WL and QD are 'switched on' where the lattice constant of the entire system is the one of Si, and the systems are relaxed a second time. The displacement vectors of the atoms in the final relaxed state are taken with respect to the pre-relaxed system thus eliminating the influence of the free surface.

The local strain tensor for each atom is computed using the calculated displacements as follows. Let $\mathrm{d}\boldsymbol{X}$ be the $3 \times N$ matrix $\mathrm{d}X_{i\alpha}$ of the distance vectors of N neighbour atoms to the atom under consideration where $i = x, y, z$ and $\alpha = 1, \ldots, N$. Given the displacement vectors of the atoms, $\mathrm{d}\boldsymbol{U}$ shall be the matrix $\mathrm{d}U_{i\alpha}$ of the differences of the displacement vectors of the neighbour atoms and the displacement vector of the centre atom. The local strain tensor is then defined as

$$\boldsymbol{\epsilon} = \mathrm{symm}(\mathrm{d}\boldsymbol{U}\,\mathrm{d}\boldsymbol{X}^{+}) \tag{1}$$

where $\mathrm{d}\boldsymbol{X}^{+} \equiv \mathrm{d}\boldsymbol{X}^{\mathrm{T}}(\mathrm{d}\boldsymbol{X}\,\mathrm{d}\boldsymbol{X}^{\mathrm{T}})^{-1}$ is the pseudo-inverse of the matrix $\mathrm{d}\boldsymbol{X}$ and symm means symmetrization. Equation (1) is the optimal solution of the equation $\boldsymbol{\epsilon}\,\mathrm{d}\boldsymbol{X} = \mathrm{d}\boldsymbol{U}$ which is the discretization of the definition of the strain tensor.

In the regions of interest in the relaxed systems, the off-diagonal part of $\boldsymbol{\epsilon}$ is negligibly small. In order to characterize the distributions of strain, we consider the planar strain $\epsilon_{\parallel} \equiv \epsilon_{xx} + \epsilon_{yy}$ and the vertical strain $\epsilon_{\perp} \equiv \epsilon_{zz}$. The strain distributions above the QD depend only weakly on h_{sub}. Unless otherwise stated, $h_{sub} = 8$ nm is chosen in the following.

3. Results of simulations

Due to the symmetries of the diamond lattice, only the range of misorientation angles $0° \leqslant \theta \leqslant 90°$ has to be considered for the tilt axis [110]. The strain distributions for the misorientation angles 0° and 13.26° will be discussed in some detail in sections 3.1 and 3.2, respectively. In section 3.3, the strain distributions for misorientation angles 54.74° and 90° will be described briefly.

3.1. Misorientation angle 0°

In this section, we consider the strain distributions in QD systems with growth direction [001], that is, there is no misorientation of the substrate. The strain distribution of a relaxed QD system typically consists of regions of tensile and compressive strain. In order to visualize the distribution, it is therefore convenient to show the surfaces of vanishing strain, or, more precisely, the atoms with nearly vanishing strain, which are the boundaries of the regions with different signs of strain. Figure 2(a) shows the surfaces of vanishing planar strain $\epsilon_{\parallel}$ of a relaxed system of size 23 nm × 23 nm × 35 nm corresponding to $h_{sub} = 3$ and $h_{SL} = 28$ nm. The surfaces resemble two bowls with bulges in the ⟨110⟩ directions. The QD is located below the lower surface. Above the QD, in between the two surfaces, $\epsilon_{\parallel}$ is positive, i.e., tensile. Immediately above the upper surface and below the lower surface, $\epsilon_{\parallel}$ is negative, that is, the lattice is compressed horizontally. The surfaces of vanishing vertical strain $\epsilon_{\perp}$ look similar; the signs of $\epsilon_{\perp}$, however, are interchanged with respect to $\epsilon_{\parallel}$.

In order to obtain a more quantitative description of the strain distribution, strain profiles along three vertical paths A, B and C the locations of which are indicated in figure 1(b) have been computed. The strain profiles for a system of size 23 nm × 23 nm × 40 nm with $h_{SL} = 28$ nm are shown in figure 2(b). Generally, the strain displays an oscillatory behaviour, as predicted by continuum elasticity calculations [5], with a strong decay with the height above the QD. Along path A, the planar strain $\epsilon_{\parallel}$ acquires the maximal value of 1.95% at the top of the QD, decreases rapidly and changes sign at height 10.9 nm above the dot. At height 15 nm, $\epsilon_{\parallel}$ has its largest negative value of −0.017% and then increases again. The vertical strain $\epsilon_{\perp}$ along path A is tensile within the dot and decays very fast above the QD to a maximal negative strain of −2.4%. It then increases and changes its sign at 8 nm above the dot, acquires a maximal value of 0.02% at 11 nm and decreases again.

Along path B, $\epsilon_{\parallel}$ has its largest negative value of −0.39% at the level of the top of the QD. It then increases and changes its sign at 8.8 nm. A second change of sign occurs at 21.5 nm. The vertical strain along path B is compressive above the WL and acquires a maximal value of 0.41%. It then decreases and oscillates with zeros at 6.7 and 19.3 nm above the height of the top of the QD.

The planar strain along path C has the maximal negative value of −0.11% at 6 nm above the height of the top of the QD. It oscillates and changes sign at 16.7 nm. The vertical strain

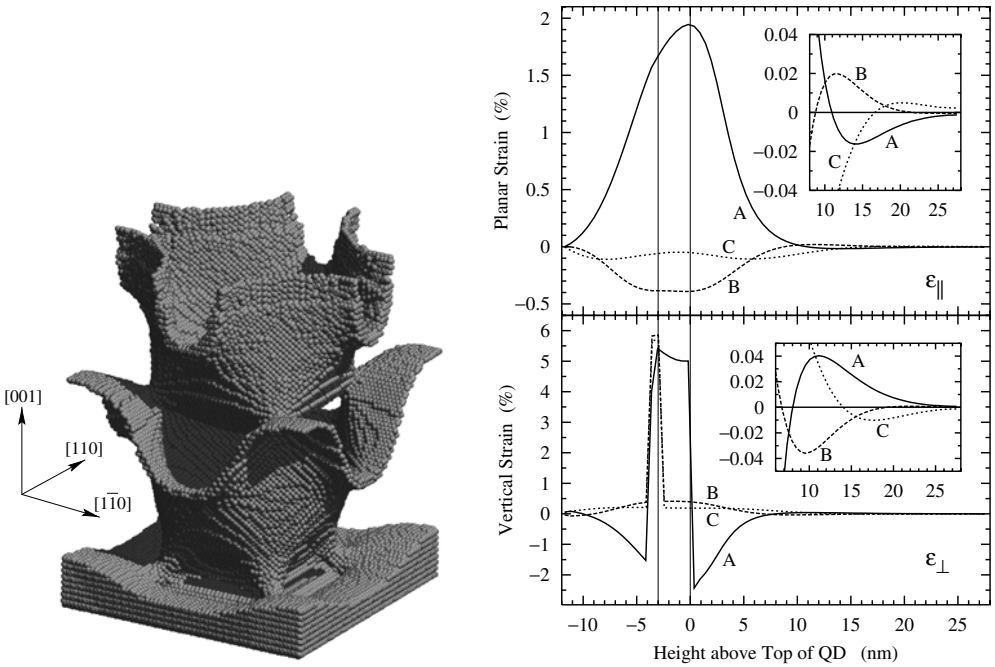

Figure 2. (a) Surfaces of vanishing $\epsilon_\parallel$ in a QD system of size 23 nm × 23 nm × 35 nm. (b) Strain profiles along three vertical paths for $\epsilon_\parallel$ and $\epsilon_\perp$ of a QD system of size 23 nm × 23 nm × 40 nm. The location of the QD is indicated by two vertical lines and the top of the QD is taken as the origin of the z-axis. The insets show the enlarged profiles for larger heights.

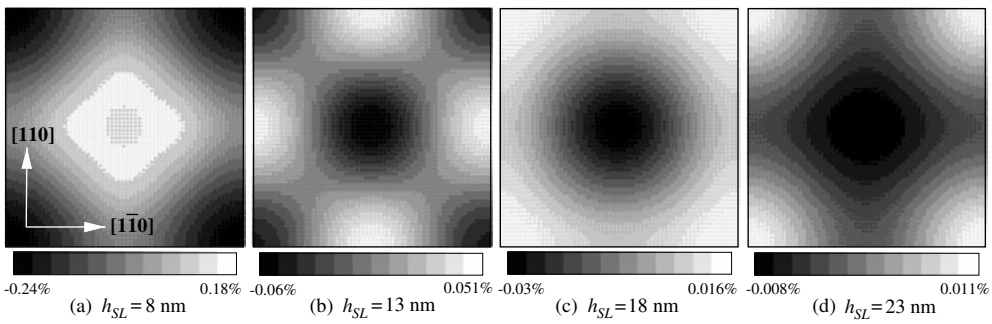

Figure 3. The strain $\epsilon_\parallel$ at the SL surface for systems with SL thicknesses 8, 13, 18 and 23 nm. The base plane has the size 23 nm × 23 nm. The greyscales are linear.

along path C has its maximal value of about 0.2% at the height of the WL. It then decreases and oscillates with a sign change at 14 nm.

In order to explain the vertical correlation of QDs in the growth of several layers of QDs, the distribution of $\epsilon_\parallel$ on the surface of the SL is relevant. Figure 3 shows the surface distributions of $\epsilon_\parallel$ of four systems with SL thicknesses of 8, 13, 18 and 23 nm. For $h_{SL} = 8$ nm, the region of tensile $\epsilon_\parallel$ is concentrated directly above the QD corresponding to a perfect vertical correlation.

Table 1. Fitted values of the parameters α, p, h and ϵ_0 for the profiles of $\epsilon_\parallel$ and $\epsilon_\perp$ along path A for $h_{SL} = 18$ nm and several widths of the simulation box.

Width (nm)	$\alpha_\parallel$	$p_\parallel$ (nm)	$h_\parallel$ (nm)	$\epsilon_{\parallel 0}$ (%)	$\alpha_\perp$	$p_\perp$ (nm)	$h_\perp$ (nm)	$\epsilon_{\perp 0}$ (%)
18.4	3.05	37.4	3.96	1.80	4.80	39.3	6.59	−2.75
23	2.86	44.9	3.99	1.92	4.55	44.4	6.41	−2.85
30	2.76	56.1	3.97	1.99	4.50	53.7	6.17	−2.86
40	2.77	79.8	3.90	2.02	4.56	70.9	5.96	−2.83
50	2.82	168	3.82	2.03	4.62	94.1	5.85	−2.79

Within this region, four positions with enlarged strain along the ⟨110⟩ directions can be seen. In the case $h_{SL} = 13$ nm, the maxima of $\epsilon_\parallel$ are located at the edges of the SL surface, that is, in between the positions of the QDs of the QD superlattice in the ⟨110⟩ directions. By further increase of h_{SL} to 18 nm, the maxima move to the corners of the surface in the ⟨100⟩ directions. These positions are even more pronounced for $h_{SL} = 23$ nm. The corresponding anticorrelation was observed in systems of CdSe QDs in a ZnSe matrix [2] and was explained by strain calculations in continuum elasticity [5, 6] where the oscillatory behaviour of the strain has been related to generalized Rayleigh waves in elastically anisotropic crystals.

In order to determine the strength of the decrease of the strain with the height above the QD, the following function was fitted to the strain profiles along path A for various box sizes.

$$\epsilon(z) = \epsilon_0 \frac{\cos[2\pi(\frac{z-z_0}{p})]}{1 + (\frac{z-z_0}{h})^\alpha}. \tag{2}$$

This functional form is chosen because it displays an oscillatory behaviour as well as a decay by a power law. The parameter p is the period of the oscillation and h may be interpreted as the height where the amplitude of the oscillation decays to half its maximal value ϵ_0 acquired at the height z_0. In the case of $\epsilon_\parallel$, $z_{\parallel 0} = 12$ nm was chosen being the location of the top of the QD. Since $\epsilon_\perp$ is discontinuous at this point, the different value $z_{\perp 0} = 9$ nm was chosen for the fitting. Table 1 contains the fitted values of the parameters α, p, h and ϵ_0 for $\epsilon_\parallel$ and $\epsilon_\perp$ in systems with $h_{SL} = 18$ nm and several lateral widths. We can see that $\epsilon_\parallel$ falls off with the power $\alpha_\parallel \approx 3$ where for large widths we have $\alpha_\parallel \approx 2.8$. The value of $h_\parallel$ for all box widths is approximately 4 nm. Except for the system of width 50 nm, the fitted value of the period $p_\parallel$ of the oscillation is about twice the box width. The deviation for the 50 nm system can be explained by the weak oscillation for the considered height of the box. For this system, the cosine in equation (2) could be set equal to unity.

The vertical strain has a decay by a power $\alpha_\perp \approx 4.6$ where the narrow box of width 18.4 nm has a stronger decay. The value of $h_\perp$ is about 6 nm for all box widths. As in the case of the planar strain, the period of the oscillation $p_\perp$ is approximately twice the box width.

For the box widths 23 and 40 nm, the simulated data and the fitted curves for $\epsilon_\parallel$ are plotted in figure 4. It can be seen that there is only a significant deviation of the simulated and fitted data at the top of the QD and some nm below the SL surface.

In order to fit function (2) to the strain profiles in systems with different heights, the base plane 30 nm × 30 nm was chosen to be fixed and h_{SL} was varied from 2 to 24 nm. For $h_{SL} \gtrsim 10$ nm, the fitted parameters do not deviate significantly from the values given in table 1. For $h_{SL} \lesssim 10$ nm, the fitting becomes increasingly inaccurate with decreasing h_{SL} which can be attributed to the boundary effects of the SL. However, function (2) can be fitted remarkably well to the values of $\epsilon_\parallel$ on the SL surface as a function of h_{SL}. The fitted parameters for $\epsilon_\parallel$ in this case are $\alpha_\parallel = 2.86$, $p_\parallel = 49$ nm, $h_\parallel = 3.8$ nm and $\epsilon_{\parallel 0} = 4.91\%$. The simulated $\epsilon_\parallel$ and

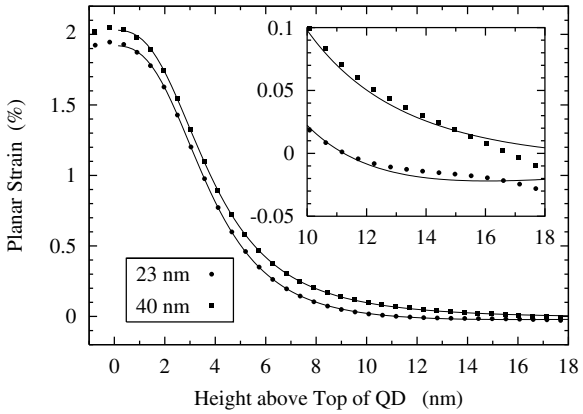

Figure 4. Simulated $\epsilon_\parallel$ and fitted curves for systems with $h_{SL} = 18$ nm and box widths 23 and 40 nm. The inset shows the enlarged data for larger values of the height.

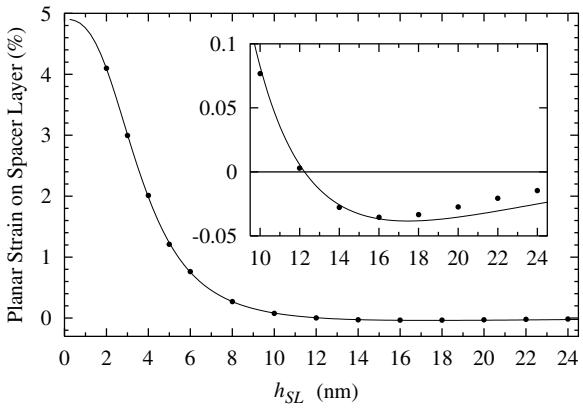

Figure 5. Simulated data and fitted curve for $\epsilon_\parallel$ at the centre of the SL surface as a function of h_{SL} for box width 30 nm × 30 nm. The inset shows the enlarged curve for larger h_{SL}.

the fitted curve are plotted in figure 5. For large h_{SL}, however, the decay of $\epsilon_\parallel$ is stronger than described by the fitted parameters.

The dependence of the period p of the strain oscillation on the system size indicates that the oscillatory behaviour is strongly influenced by the lateral environment of a QD. Table 1 shows that the oscillations persist at least up to a superlattice constant three times the width of the dot. The oscillatory behaviour also depends on the number of neighbouring dots. In all QD systems considered so far in this article, the number of nearest neighbour QDs has been four. To see the dependence of $\epsilon_\parallel$ on the coordination number of the QD superlattice, simulations with two, three and six nearest neighbours have additionally been performed. In the first case, a simulation box with box length in the y-direction more than twice the length in the x-direction has been chosen. For the last two cases, simulation boxes with a parallelogram as base plane have been chosen where for the coordination number three, two dots have been taken into the simulation box. In all simulations, the distance between the dots is about 23 nm and $h_{SL} = 28$ nm. The fitted parameters $\alpha_\parallel$, $p_\parallel$ and $h_\parallel$ along a vertical path through the centre of the QDs for the fitting function (2) are collected in table 2. The fitted value of $\epsilon_{\parallel 0}$ for all cases is 2%. It can be seen that the parameters $\alpha_\parallel$ and $h_\parallel$ are nearly independent of the number

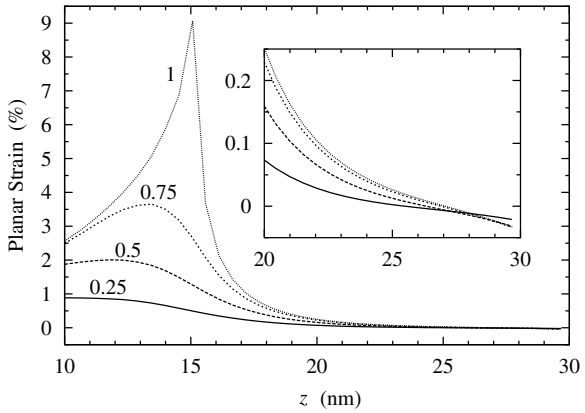

Figure 6. Simulated $\epsilon_\parallel$ along path A for systems of size 30 nm × 30 nm × 30 nm and several heights of truncation of the QD pyramids. The inset shows the enlarged strain curves for larger height.

Table 2. Fitted values of the parameters $\alpha_\parallel$, $p_\parallel$ and $h_\parallel$ for strain profiles along a vertical path through the centre of the QDs in QD systems with different coordination numbers of the QD superlattice.

Coordination number	$\alpha_\parallel$	$p_\parallel$ (nm)	$h_\parallel$ (nm)
2	2.95	83.9	3.81
3	2.85	56.7	3.95
4	2.92	45.2	3.99
6	2.87	43.0	4.08

Table 3. Fitted values of the parameters $\alpha_\parallel$, $p_\parallel$, $h_\parallel$ and $\epsilon_{0\parallel}$ for profiles of $\epsilon_\parallel$ along path A for different heights of truncations of the QD pyramids in systems of size 30 nm × 30 nm × 30 nm.

Height of truncation	$\alpha_\parallel$	$p_\parallel$ (nm)	$h_\parallel$ (nm)	$\epsilon_{\parallel 0}$ (%)
0.25	3.06	58.1	5.52	0.88
0.5	2.76	56.1	3.97	1.99
0.75	2.45	56.0	2.43	3.59
1	1.24	42.8	0.38	10.2

of neighbouring dots. The period of the oscillation $p_\parallel$ shows a decrease from 84 nm for two neighbours to 43 nm for six neighbours where in the cases of four and six neighbours the periods are nearly equal.

To gain insight into the dependence of the strain distribution on the form of the QD, simulations have been performed with dots that are truncated at factors 0.25, 0.5, 0.75 and 1 of the height of a pyramid. The truncation height 0.5 corresponds to the case considered so far in this paper. Figure 6 shows the profiles of $\epsilon_\parallel$ along path A for systems of size 30 nm × 30 nm × 30 nm. The behaviour of $\epsilon_\parallel$ for the different truncations is similar to that found in [17] by means of analytical computations for elastically isotropic materials. Equation (2) has been fitted to the profiles in figure 6 where $z_{0\parallel}$ is chosen to be the height of the top of the truncated pyramids. From the fitted parameters given in table 3, it can be seen that for truncation factors $\leqslant 0.75$ the parameters $\alpha_\parallel$, $h_\parallel$ and $p_\parallel$ depend only weakly on the form of the dot. The large variation of $\epsilon_{0\parallel}$ can be attributed to the different dot volumes. In the case

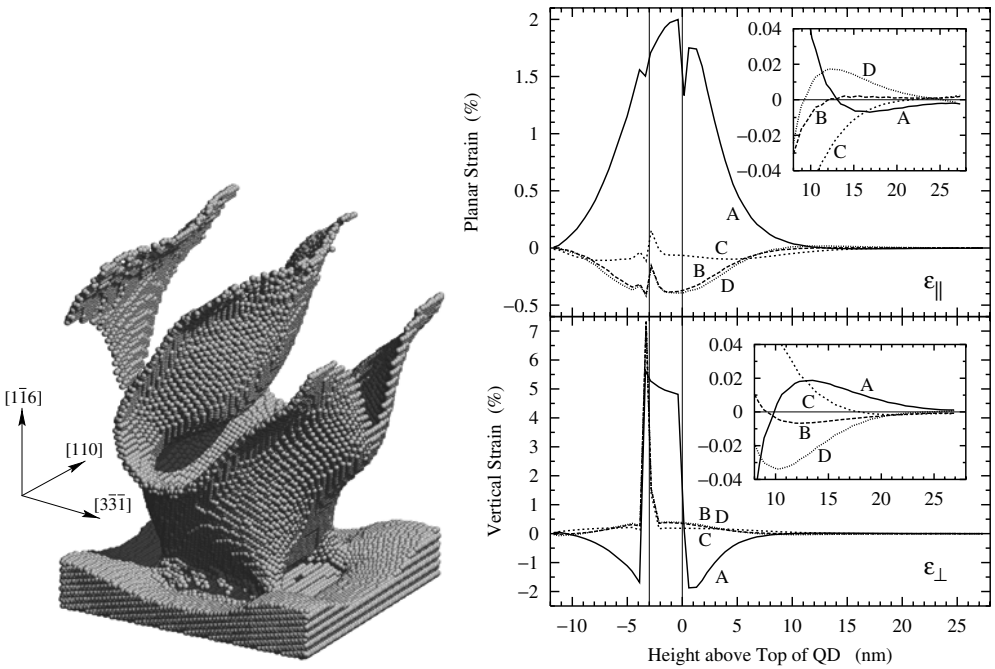

(a) (b)

Figure 7. (a) Surfaces of vanishing $\epsilon_{\parallel}$ in a QD system of size 23.7 nm × 23 nm × 35 nm and misorientation angle 13.26°. (b) Strain profiles along four vertical paths in a QD system of size 23.7 nm × 23 nm × 40 nm and misorientation angle 13.26°. The location of the QD is indicated by two vertical lines and the top of the QD is taken as the origin of the z-axis. The insets show the enlarged profiles for larger height.

of the pyramid-shaped dot, the decay of $\epsilon_{\parallel}$ corresponds nearly to an inverse linear function as was found for the hydrostatic stress above a pyramidal QD [8].

3.2. Misorientation angle 13.26°

In this section, we discuss the strain distributions in QD systems with a misoriented lattice which means that the growth direction is different from the [001] direction. The fixed misorientation angle 13.26° is chosen, which corresponds to the substrate plane (1$\bar{1}$6). The typical strain distribution in a system with base plane of 23.7 nm × 23 nm, $h_{sub} = 3$ and $h_{SL} = 28$ nm is visualized in figure 7(a) where the surfaces of vanishing $\epsilon_{\parallel}$ are shown. It can be seen that by tilting the growth direction, the surfaces of the two bowls in figure 2(a) merge to form an inclined tube that is connected to the tubes of the neighbouring QDs in the [110] direction. The region of tensile $\epsilon_{\parallel}$ located above the QD is inclined in the direction opposite to the misorientation.

As in the case of the QD with misorientation 0°, the strain profiles along several paths in the system have been computed. The profiles of $\epsilon_{\parallel}$ and $\epsilon_{\perp}$ for paths A, B, C and D are plotted in figure 7(b). The simulation box has the size 23.7 nm × 23 nm × 40 nm with $h_{SL} = 28$ nm. The large variations of $\epsilon_{\parallel}$ at the WL and at the top of the QD are due to the lattice misorientation and the ensuing steps in the Si–Ge interfaces which cause an extra planar strain. The strain

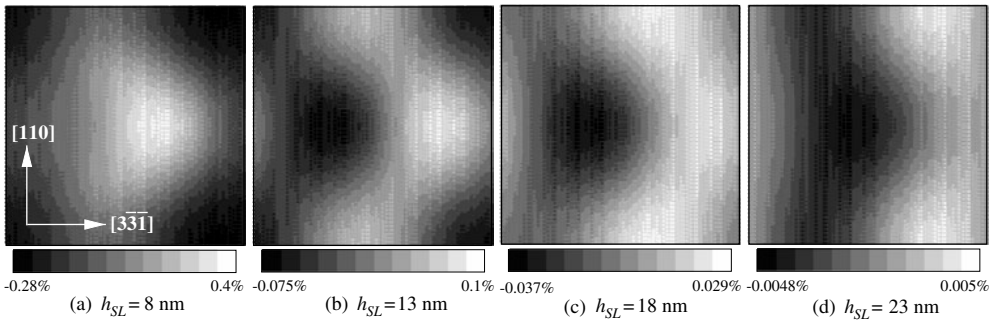

Figure 8. The strain $\epsilon_\parallel$ at the SL surface for systems with misorientation 13.26° and SL thicknesses 8, 13, 18 and 23 nm. The size of the base plane is 23.7 nm × 23 nm. The greyscales are linear.

distribution of the misoriented system is similar to the one of the system with growth direction [001] shown in figure 2(b). However, the strain along paths B and C of the misoriented system has a stronger decay than in the case of the system without misorientation which means that the strain is concentrated in the region above the QD and at the borders of the box in the [110] direction. Since the strain distribution in the misoriented system is asymmetric, there exists no preferred path for which function (2) could be fitted to the corresponding strain profiles to give representative data of the profiles.

In order to investigate the distribution of $\epsilon_\parallel$ as a function of h_{SL}, simulations have been performed with SL thicknesses 8, 13, 18 and 23 nm. Figure 8 shows the distribution of $\epsilon_\parallel$ on the SL surface. For $h_{SL} = 8$ nm, the maximum of $\epsilon_\parallel$ is displaced from the centre in the [3$\bar{3}\bar{1}$] direction by 1.9 nm. In the case of $h_{SL} = 13$ nm, this maximum is displaced by 6.6 nm and there appear regions of positive $\epsilon_\parallel$ between the locations of QDs in the superlattice of QDs in the [110] direction. In the negative [3$\bar{3}\bar{1}$] direction, a maximum of compressive strain appears. For $h_{SL} = 18$ nm, the region of tensile $\epsilon_\parallel$ is spread out over a band floating around the maximum of compressive $\epsilon_\parallel$. Eventually, for $h_{SL} = 23$ nm, there are only maxima of positive $\epsilon_\parallel$ at the edges in the [110] direction which are displaced in the [3$\bar{3}\bar{1}$] direction by 7.6 nm. Thus, it is to be expected that in the growth of three-dimensional QD superlattices there occurs a vertical correlation where the QDs in successive layers are displaced in the direction opposite to the misorientation. This behaviour was first predicted in [6] and found experimentally in [4]. It should be noted that the side maxima in figures 8(b)–(d) correspond to the maxima at the edges of the system in figure 3(b) for the case of the misorientation 0°. The maxima at the corners of the SL in figures 3(c) and (d) are not present in the misoriented system.

Next, we consider the dependence of the strain distribution on the size of the base plane. The strain profiles for QD systems of fixed h_{SL} and different lateral sizes are very similar to the ones for the untilted systems. This means that for two-dimensional QD superlattices with increasing superlattice constant, the regions of tensile strain above the QDs get more compact and the periods of the strain oscillations in the vertical direction increase. This can be seen more clearly by considering the location of the regions of tensile $\epsilon_\parallel$ as a function of the height above the QD. To this end we define the moment $\hat{x}$ of $\epsilon_\parallel$ in the x-direction by

$$\hat{x}(z) = \frac{\sum_{\epsilon_\parallel > 0} x \epsilon_\parallel(z)}{\sum_{\epsilon_\parallel > 0} \epsilon_\parallel(z)}. \tag{3}$$

The summations are performed over all atoms with positive $\epsilon_\parallel$ in a thin layer at height z. The resulting curves for six different system widths are plotted in figure 9 where $h_{SL} = 18$ nm

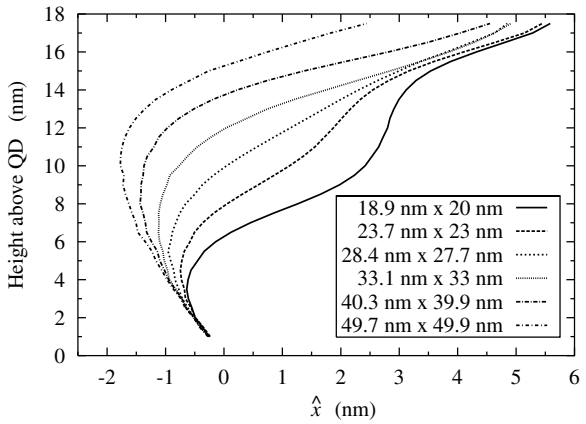

Figure 9. The moment $\hat{x}$ of the positive planar strain as a function of the height above the QD for different box widths.

and where the centre of the QD is taken as the origin of the x-axis. The values of the moment $\hat{y}$ of $\epsilon_{\parallel}$ in the y-direction are for all systems located directly above the QD as expected for symmetry reasons. From figure 9 we see that with increasing height $\hat{x}$ is bent in the direction opposite to the misorientation where in the case of small box width there is a second bend in the negative x-direction for larger height. The reasons for this are the maxima of $\epsilon_{\parallel}$ at the sides of the box which dominate $\hat{x}$ for large z-values. These maxima are absent for larger box widths. In figure 9 we also see that the values of $\hat{x}$ at the SL surface decrease with increasing box widths.

In order to determine the correlation of QDs in consecutive layers of QDs as a function of h_{SL}, a series of simulations has been performed with systems of different heights where a fixed box width of 40.2 nm $\times$ 39.9 nm has been chosen. In this case, the maxima of tensile $\epsilon_{\parallel}$ at the sides of the systems in the [110] direction are only weak while the regions of positive $\epsilon_{\parallel}$ in the middle of the system are pronounced even for large h_{SL} up to 23 nm. On the surface of the SL, the position of maximal $\epsilon_{\parallel}$ has been determined. In the y direction, this position always lies approximately in the middle of the system. From the x value of the maximum, the correlation angle γ with respect to the top of the QD has been computed. The values of γ as a function of h_{SL} are plotted in figure 10. For small h_{SL}, the correlation angle is negative which means that the displacement of the strain maximum is in the direction of the misorientation. For larger h_{SL}, the displacement is in the opposite direction and it acquires an asymptotic value of about 25°. The intermediate maxima of the correlation angle may be due to the boundary conditions of the QD superlattice.

The behaviour of the correlation angle shown in figure 10 stands in contrast to the one found experimentally. For a system of InP QDs in GaInP matrix, an increase of the correlation angle for decreasing h_{SL} was found in misoriented samples [4]. Indeed, at least for length scales where h_{SL} is comparable to the QD height, the strain distribution on the SL surface cannot be the sole reason for the vertical correlation in the case of a misorientation.

3.3. Misorientation angles 54.74° and 90°

Simulations of the strain distributions for several misorientation angles in the range $0° \leqslant \theta \leqslant 90°$ have been performed. The most interesting cases, apart from the ones considered in the previous sections, are the tilt angles 54.74° and 90° corresponding to the growth planes (111)

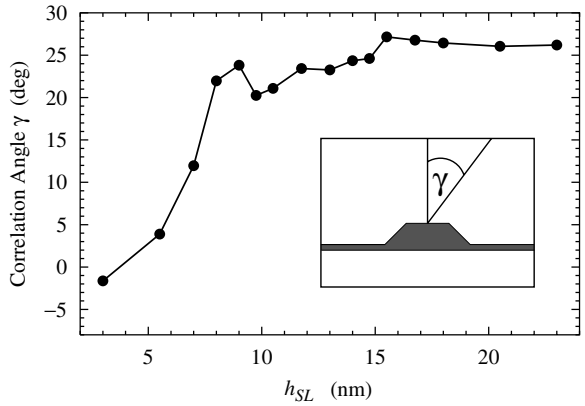

Figure 10. The correlation angle γ as a function of h_{SL} for a system of width 40.3 nm × 40 nm and lattice misorientation 13.26°.

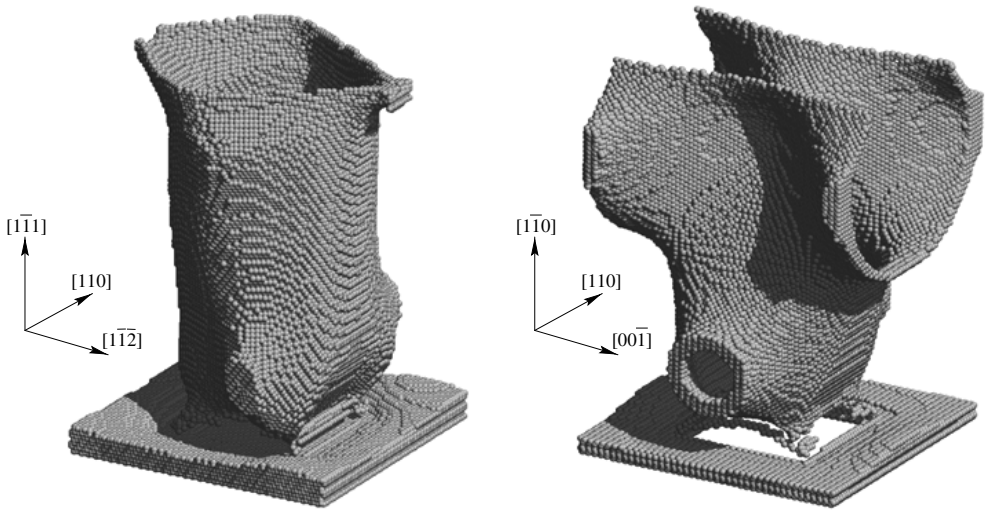

(a) θ = 54.74° (b) θ = 90°

Figure 11. Surfaces of vanishing $\epsilon_{\parallel}$. (a) (1$\bar{1}$1) base plane with system of size 22.6 nm × 23 nm × 35 nm, (b) ($\bar{1}$10) base plane with system size 22.8 nm × 23 nm × 35 nm.

and (110), respectively. The surfaces of vanishing $\epsilon_{\parallel}$ for these systems are shown in figure 11 where $h_{sub} = 3$ and $h_{SL} = 28$ nm.

In the case of the misorientation angle 54.74°, the tilted tube in the system with misorientation 13.26° shown in figure 7 has developed into a tube that lies along the growth direction [1$\bar{1}$1] with only a small broadening at the top of the SL. The tensile $\epsilon_{\parallel}$ inside the tube is thus concentrated into a narrow region which should produce a perfect vertical correlation in QD superlattices. Function (2) has been fitted to $\epsilon_{\parallel}$ along path A for several widths of the base plane. For the exponent $\alpha_{\parallel}$, the value 1.7 was obtained. The parameter $h_{\parallel}$, however, has the small value 1.7 nm. The period $p_{\parallel}$ of the oscillation for a box of width 24 nm is about 150 nm, while in the case of width 35 nm the cosine in equation (2) can be set equal to unity. This demonstrates that there is almost no oscillation of $\epsilon_{\parallel}$.

For the misorientation angle 90°, we can see from figure 11(b) that there is a strong variation of $\epsilon_{\parallel}$ with the height above the QD giving rise to several possible forms of correlation of QDs where the lateral direction [001] is a preferred direction. In the [110] direction, horizontal necks emerge connecting the regions of tensile $\epsilon_{\parallel}$ above dots in the QD superlattice where the beginnings of the lower necks can already be seen in figure 11(a).

4. Conclusions

In this paper, I have presented results of large-scale atomistic simulations of strain distributions in Ge/Si QD systems using the Tersoff interatomic potential. The strain fields outside the QDs have been studied as a function of the system width and height as well as of the substrate misorientation angle. The main aim of this work was the explanation of different vertical correlations of QD superlattices by the strain distributions on the SL. Some results obtained within the continuum theory of elasticity given previously in the literature are confirmed, refined and extended.

The simulated strain distributions generally show an oscillatory behaviour outside the QD with a strong decay with increasing distance from the QD. Several methods have been applied in this article to characterize the strain distributions: the surfaces of vanishing strain and the two-dimensional strain distributions on the SL have been visualized. The strain profiles along selected vertical lines have been analysed where a simple fitting function was used to quantify the period of the oscillation and the strength of the decay of the strain. The period of the oscillation is nearly proportional to the spacing of the QDs in the effective two-dimensional superlattice of QDs and the period decreases with increasing number of neighbouring dots. Thus, a high two-dimensional density of QDs should favour an anticorrelation in the growth of three-dimensional QD superlattices. The strength of the decay of the strain above a QD depends on the form of the QD. For truncated pyramids that are not too peaked, a decay of the planar strain by approximately r^{-3} was found. This corresponds to the well known -3 power law for a spherical inclusion obtained in isotropic elasticity theory. In the singular case of a perfect pyramid, the decay proceeds by nearly r^{-1}. In the case of misoriented systems with small misorientation angles, two effects of the elastic anisotropy can be discerned: first, the region of tensile $\epsilon_{\parallel}$ above the QD is bent in the direction opposite to the misorientation causing a shift in the vertical correlation of QDs, and secondly, the vertical oscillations lead to an anticorrelation which is different from the one for the systems without misorientation. For systems misoriented by 13.26° with a large horizontal distance of QDs where the anticorrelation is weak, the correlation angle corresponding to the lateral shift of the strain tends with increasing SL thickness towards the asymptotic value $\approx$25°. An optimal vertical correlation should be obtained for the misorientation angle 54.74° corresponding to the growth plane (111) since in this case the region of positive planar strain is strongly concentrated above the QD.

Acknowledgments

I would like to thank H-R Trebin, A Fantini, F Gähler and F Scholz for helpful discussions. This work was supported by the Deutsche Forschungsgemeinschaft (DFG) within the Graduiertenkolleg ‘Interfaces in crystalline materials’ (GRK 285). The simulations were performed on the Cray T3E of the High Performance Computing Center Stuttgart.

References

[1] Xie Q, Madhukar A, Chen P and Kobayashi N P 1995 *Phys. Rev. Lett.* **75** 2542
[2] Strassburg M, Kutzer V, Pohl U W, Hoffmann A, Broser I, Ledentsov N N, Bimberg D, Rosenauer A, Fischer U, Gerthsen D, Krestnikov I L, Maximov M V, Kop'ev P S and Alferov Z I 1998 *Appl. Phys. Lett.* **72** 942
[3] Springholz G, Holý V, Pinczolits M and Bauer G 1998 *Science* **282** 734
[4] Fantini A, Phillipp F, Kohler C, Porsche J and Scholz F 2002 *J. Cryst. Growth* **244** 129
[5] Shchukin V A, Bimberg D, Malyshkin V G and Ledentsov N N 1998 *Phys. Rev.* B **57** 12262
[6] Holý V, Springholz G, Pinczolits M and Bauer G 1999 *Phys. Rev. Lett.* **83** 356
[7] Kikuchi Y, Sugii H and Shintani K 2001 *J. Appl. Phys.* **89** 1191
[8] Makeev M A and Madhukar A 2001 *Phys. Rev. Lett.* **86** 5542
[9] Daruka I, Barabási A-L, Zhou S J, Germann T C, Lomdahl P S and Bishop A R 1999 *Phys. Rev.* B **60** R2150
[10] Yu W and Madhukar A 1997 *Phys. Rev. Lett.* **79** 905
Yu W and Madhukar A 1997 *Phys. Rev. Lett.* **79** 4939 (erratum)
[11] Pryor C, Kim J, Wang L W, Williamson A J and Zunger A 1998 *J. Appl. Phys.* **83** 2548
[12] Scheerschmidt K, Conrad D, Kirmse H, Schneider R and Neumann W 2000 *Ultramicroscopy* **81** 289
[13] Balamane H, Halicioglu T and Tiller W A 1992 *Phys. Rev.* B **46** 2250
[14] Tersoff J 1989 *Phys. Rev.* B **39** 5566
[15] Sakamoto K, Matsuhata H, Tanner M O, Wang D and Wang K L 1998 *Thin Solid Films* **321** 55
[16] Rastelli A, Kummer M and von Känel H 2001 *Phys. Rev. Lett.* **87** 256101
[17] Pearson G S and Faux D A 2000 *J. Appl. Phys.* **88** 730